Materials Science-Poland, 39(4), 2021, pp. 615-625
http://www.materialsscience.pwr.wroc.pl/
DOI: 10.2478/msp-2022-0002

Decomposition mechanisms of continuously cooled bainitic rail in the critical heat-affected zone of a flash-butt welded joints

Aleksandra Królicka[1,*], Andrzej Żak[2], Roman Kuziak[3], Krzysztof Radwański[3], Andrzej Ambroziak[1]

[1]Department of Metal Forming, Welding and Metrology, Wroclaw University of Science and Technology, Wybrzeże Wyspiańskiego 27, 50-370 Wroclaw, Poland

[2]Faculty of Mechanical Engineering, Wroclaw University of Science and Technology, Wybrzeże Wyspiańskiego 27, 50-370 Wroclaw, Poland

[3]Łukasiewicz Research Network – Institute for Ferrous Metallurgy, K. Miarki 12-14, 44-100 Gliwice, Poland

The joining process of bainitic rails is significant in terms of their industrialization in high-speed and heavy-loaded railways. This paper demonstrates the microstructure changes in the critical zone of the welded joint, which is responsible for the greatest deterioration in mechanical properties. Extensive progress in the decomposition of the retained austenite and bainitic ferrite occurs in the low-temperature heat-affected zone (LTHAZ) of the flash-butt welded joint of low-carbon bainitic rail. The decomposition products of the retained austenite were mainly a mixture of cementite and ferrite. The cementite was mainly precipitated at the boundary of the bainitic ferrite laths, which indicates lower thermal stability of the filmy austenite. Moreover, it was found that a part of the refined blocky retained austenite was decomposed into the ferrite and nanometric cementite, while another remained in the structure. The decomposition mechanisms are rather heterogeneous with varying degrees of decomposition. A relatively high proportion of dislocations and stress fields prove the occurrence of residual stresses formed during the welding process.

Keywords: *bainite, rails, HAZ, welded joints, welding, retained austenite, austenite decomposition, cementite, TEM study, residual stresses, softening zone*

1. Introduction

In recent years, the issue of the possibility of using bainitic steels in the railway industry has been the subject of extensive research. In just 2 years, significant research reports have been published in terms of low-carbon bainitic steels intended for applications in railway infrastructure. The latest investigations cover a wide range of issues including microstructure optimization considering alloying additives [1] and processing techniques [2]; manufacturing process [3]; heat treatments methods [4]; wear resistance [5]; rolling contact fatigue [6]; low-cycle fatigue performance [7]; fatigue crack growth rate [8]; and analysis of welding processes [9]. The mechanical properties of bainitic steels, compared with those of conventional ones, are promising and indicate the possibility of enhancing the durability of railway tracks, especially under heavy loads. However, some controversies and ambiguities in the evaluation of the advantage of bainitic rails over pearlitic rails have been significantly noticeable.

Several studies in the literature address the issue of the welding process of high-strength multiphase steels. Morawiec et al. [10] attempted to assess the impact of laser welding parameters on TRIP-assisted advanced high-strength steel (AHSS). Fang et al. [11] proposed the dedicated welding method for nanoscale bainitic steels. Królicka et al. [12] compared the regeneration technique with the post-welding heat treatment (PWHT) of a commercial steel, 55Si7, with a refined multiphase structure. Wang and Speer [13] performed the welding process on commercial QP980 steel after quenching and partitioning (Q&P) heat treatment. In these

* E-mail: aleksandra.krolicka@pwr.edu.pl

© A. Królicka et al. 2021. This is an open access article distributed under the Creative Commons Attribution-NonCommercial-NoDerivatives 4.0 License. (http://creativecommons.org/licenses/by-nc-nd/4.0/)

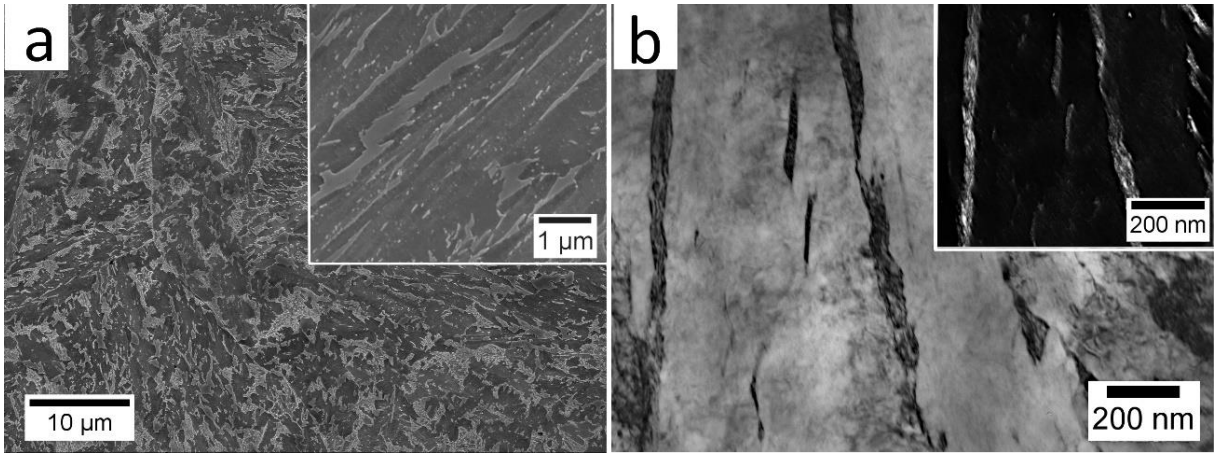

Fig. 1. Microstructure of base material of bainitic rails. **(A)** Visible lath morphology of bainitic ferrite, blocky and film-like retained austenite, and cementite precipitations inside bainitic ferrite laths. Scanning Electron Microscopy, 15 kV, secondary electrons detector. **(B)** Bright-field image of bainitic ferrite and austenite films. Dark-field image obtained from retained austenite reflex. Transmission Electron Microscopy, 150 kV

tests, they applied the resistance spot welding, laser welding, and MAG methods. The results of these investigations indicate that welding processes in relation to high-strength multiphase steels are influenced by many factors related to the various phase contributions.. Retained austenite and its thermal stability play a crucial role in terms of welding processes of multi-phase steels Thus, the kinetics of phase transformations of different types of multiphase steels cannot be directly compared and require individual assessment. This fact was the motivation for a detailed analysis of the decomposition processes of low-carbon bainitic steels after continuous cooling processes relevant to the specified heat-affected zone, which is responsible for the highest decrease in hardness.

The welding of bainitic rails is relatively poorly known in terms of the metallurgical changes occurring during this process. In a previous work [9], the authors analyzed the changes in the microstructure occurring in the flash-butt welded joint of low-carbon, continuous cooled bainitic steel. It should be emphasized that this welding method is typical for conventional rail joining. In this research, the mechanisms of austenite decomposition and bainite degradation occurring in the low-temperature heat-affected zone (LTHAZ) of the welded joints of the bainitic rail were determined in detail. This zone was defined as critical in the context of the lowest hardness and adverse microstructure morphology. Moreover, the highest degree of microstructure degradation concerning the parent material was found. The LTHAZ is also called the softened zone, which is the most crucial problem in the case of welded joints of high-strength steels. However, this research is focused on identifying complex degradation mechanisms and morphological changes using high-resolution transmission electron microscopy (HRTEM). Understanding the microstructural changes in this zone may allow for future optimization of welding processes with a reduction of this adverse morphology of microstructure. Considering the complex nature of decomposition mechanisms, this research will provide a better explanation of the processes responsible for causing an adverse microstructure morphology, and complement previous findings pertaining to bainite transformation in the literature.

2. Materials and methods

For this investigation, multiphase rail steel with the chemical composition of 0.28% C, 1.1% Si, 2.5% (Mn + Cr), and small additions of Ni and Mo were subject to the flash-butt welding process. The motivation for designing this material was the

need to identify a bainitic steel suitable for deployment in high-speed and heavy-loaded railway applications. The tested bainitic rail was subjected to a continuous cooling process directly after the manufacturing process. The silicon content significantly inhibited cementite precipitations; however, a limited number of these precipitates was identified. The base material microstructure consisted of bainitic ferrite, retained film-like austenite, retained blocky austenite, and a low fraction of cementite precipitations (Figure 1).

The rails with the standard 60E1 profile were subjected to welding using the flash-butt welding method. This method of welding includes the joining process of molten parts applying the resistance heating, and simultaneous compressive force. An industrial resistance welding machine was utilized to perform welding process. The detailed welding process parameters are provided in Królicka et al. [9]. It should be mentioned that the performed welding process was conducted in the field, with industrial conditions being in accordance with the standard joining conditions.

The zone considered in this work is marked in yellow in Figure 2. The LTHAZ is a zone affected by an elevated temperature associated with the welding process, which was higher than the bainite transformation but lower than the maximum temperature of the ferrite stability (i.e., A_{c1}). Thus, there was no inverse transformation to austenite in this region, and the entire region was characterized by the parent multiphase structure subjected to degradation processes. The zone was characterized by the lowest level of hardness (approx. 275 HV10) concerning the base material (approx. 385 HV10), as indicated in Figure 2.

The base material was observed using a JEOL JSM-7200F (Japan, Tokyo) scanning electron microscope after etching with 3% nital (a solution of nitric acid, HNO_3, and ethanol), and using a topographic contrast mode (secondary electrons [SE] detector) and an accelerating voltage of 15 kV. An electron backscattered diffraction method (EBSD) was also applied (EDAX detector, AMETEK, Berwyn, PA, U.S.). These observations were carried out in areas of 25.3 μm× 25.4 μm, with a step size of 60 nm. The data obtained during

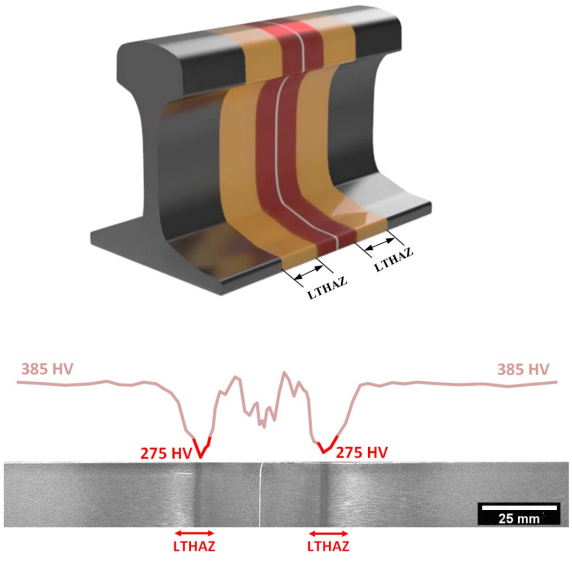

Fig. 2. The model of flash-butt welded joints (the area subjected to investigations is marked in yellow) and the hardness distribution of the welded joint with the distinguished tested LTHAZ area. Hardness was measured by the Vickers method with a load of 98.1 N (HV10). LTHAZ, low-temperature heat-affected zone

analysis were processed employing TSL software (OIM Analysis™ 8, Berwyn, PA, USA). A confidence index standardization and single iteration grain dilation clean-up procedures were adjusted for each analysis. A grain tolerance angle of 5° was assumed for grain size data. The minimum grain size was adapted as 2 pixels. The clean-up procedure affected less than 5% of all measurement pixels. Observations of LTHAZ were carried out using the Hitachi H-800 (Tokyo, Japan) transmission electron microscope and JEOL JEM-F200 (Tokyo, Japan) high-resolution electron microscope. Samples having a thickness of approximately 1.2 mm were cut using the precision electro-erosive method from the selected zone of the welded joint. Sample preparation also included mechanical pre-thinning to a thickness of approximately 80 μm. Subsequently, discs with a diameter of 3 mm were cut out by mechanical method. Afterward, electrochemical polishing and ion polishing were applied using Struers TenuPol (Cleveland, U.S.) and the GATAN DuoMill (Berwyn, PA, U.S.), respectively.

The portable μ-X360s X-ray analyzer (PULSTEC Industrial Co., Ltd., Japan) was used to measure the residual stress distribution of welded joints. The determination of welding residual stresses was conducted by the $\cos\alpha$ method. The detector gun of the analyzer was inclined at an angle of 35°. The dedicated software was also utilized (version. 2.5.6.0). A continuous Debye–Scherrer ring was detected during 60 s. The measurements included various zones of a welded joint (FZ – fusion zone, HTHAZ - high-temperature heat-affected zone, the area between HTHAZ and LTHAZ, LTHAZ, and BM – base material), where at least three repetitions were performed.

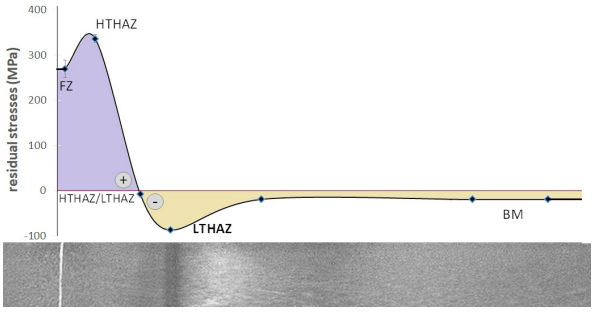

Fig. 3. The residual stresses' distribution in the tested welded joint: (+) tensile residual stresses, (−) compressive residual stresses. LTHAZ, low-temperature heat-affected zone

3. Results and discussion

In view of the welding processes, the evaluation of welding residual stresses is significant due to the need for ensuring high mechanical properties and durability [14]. It is well known that compressive residual stresses increase and tensile residual stresses decrease in the fatigue strength [15]. The nature of the residual stress distribution depends primarily on the welding process parameters, welding method, material chemical composition, and the undergoing phase transformations [16]. The flash-butt welded bainitic steel is characterized by a typical residual stress distribution (Figure 3). The maximum measured tensile stresses were approximately 340 MPa at the HTHAZ, which did not exceed half the yield strength of the tested material (780 MPa). However, compressive stresses occurred in the critical LTHAZ (approx. −90 MPa), which were higher than that in the base material (−20 MPa). It can also be assumed that the slight compressive stresses in the base material are related to the bainite transformation occurring during the manufacturing process [17]. It should be highlighted that the occurrence of compressive stresses in the LTHAZ is not a negative feature in the context of fatigue properties, but may have an important impact on the mechanisms of microstructure decomposition. Details of the microstructures of other zones of the same material as was tested in the present study are available elsewhere in the literature [9].

The quasi-quantitative evaluation of the LTHAZ (Figure 4D–4F) compared with the base material (Figure 4A–4C) was performed using the EBSD method. Severe changes in the microstructure were found, which, after the welding process, did not contain a distinct lath morphology of bainitic ferrite (Figure 4A and 4D). There were also differences in the content of retained austenite (Figure 4B and 4E), which confirms that in the LTHAZ, it was almost completely decomposed. This is also accompanied by the various distribution of misorientation angles. In the case of the base material, the typical angles for the K-S; Kurdjumov-Sachs (42.85°) and N-W; Nishiyama-Wasserman (45.99°) orientation relationships prevailed (Figure 4C). The lack of the typical K-S and N-W orientations in the LTHAZ is associated with the decomposition of the retained austenite. The LTHAZ was characterized by the domination of 50°–60° misorientation angles, high angle boundaries (HABs), and an increased fraction of low angle boundaries (LABs), as indicated in Figure 4F. The HABs correspond to ferrite boundaries (visible in Figure 4D and 4E as bold black lines at the bainitic ferrite boundaries), while LABs in the range of 2.5°–8° probably refer to areas inside the bainitic ferrite that can be attributed to the formation of subgrains [18]. Increasing the fraction of LABs is related to the processes of retained austenite decomposition.

Overall, bainitic ferrite and retained austenite during tempering processes at sufficiently high

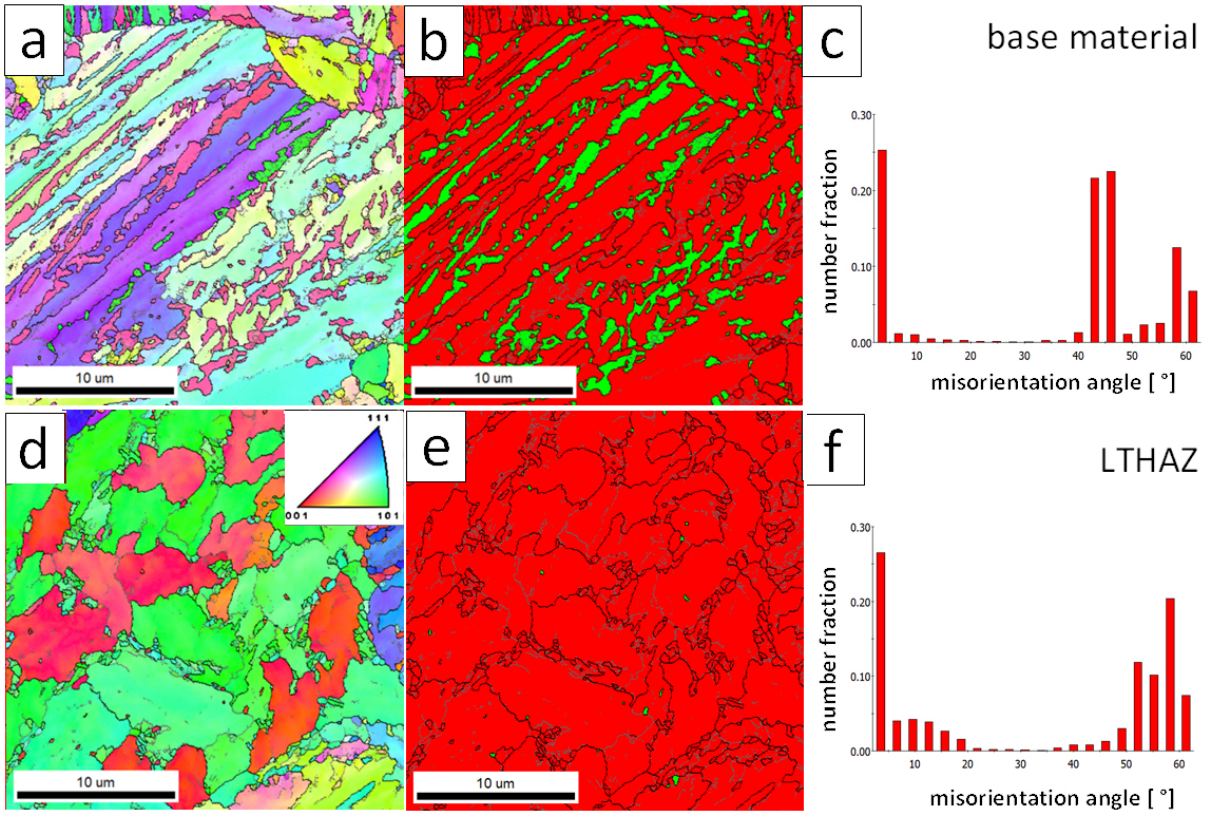

Fig. 4. Comparison of inverse pole figure maps **(A, D)** and phase distribution maps **(B, E)** – retained austenite marked in green, bainitic ferrite marked in red, and misorientation distributions **(C, F)** between the base material and the LTHAZ indicated. LTHAZ, low-temperature heat-affected zone

Table 1. The comparison of the critical LTHAZ and tempering process of bainitic steels

Microstructural feature or decomposition mechanism	**LTHAZ (this study)**	**Severe tempering process [30]**
Hardness drop	Occur	Occur
Retained austenite decomposition	$\gamma_{RA} \rightarrow \alpha + \theta$	$\gamma_{RA} \rightarrow \alpha + \theta$ $\gamma_{RA} \rightarrow \alpha' \mid$ M/A $\gamma_{RA} \rightarrow$ P
Nature of retained austenite decomposition	Heterogeneous (combination of indirect and direct approaches)	Direct approach
Dislocation	Occur together with Moiré fringes and stress fields	Dislocation relaxation
Precipitation coarsening	Occur	Occur

γ_{RA}, retained austenite; α, ferrite; θ, cementite; α', martensite; LTHAZ, low-temperature heat-affected zone; M/A, martensite/austenite constituents; P, pearlite.

temperatures are degraded into a mixture of cementite and ferrite [19]. The LTHAZ affected by the temperature below Ac_1 can be compared to the rapid tempering processes [20]. Thus, the decomposition mechanisms should be comparable to the tempering processes. Retained austenite during tempering decomposes into a mixture of cementite and ferrite ($\gamma_R \rightarrow \alpha + \theta$) [21]. There

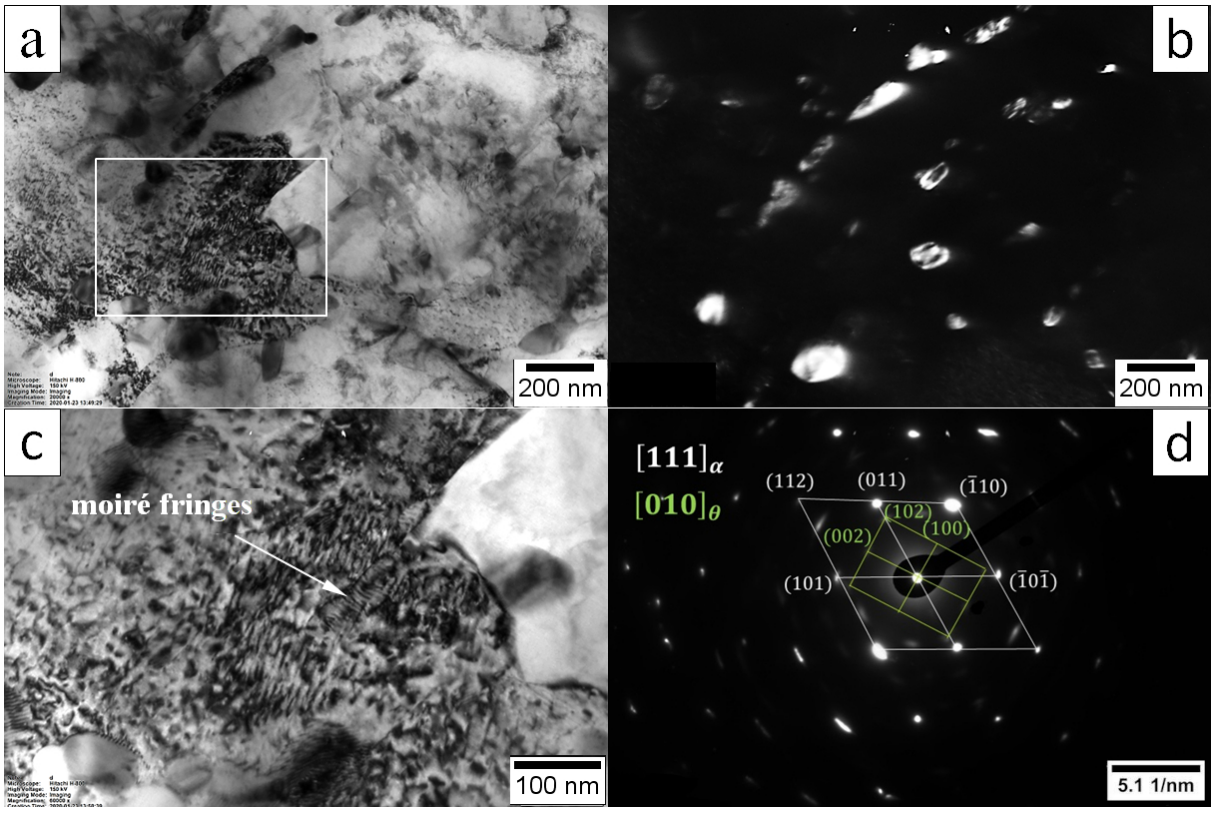

Fig. 5. **(A)** Bright-field image of LTHAZ and **(B)** corresponding dark-field image from cementite precipitations. **(C)** The magnification of the area marked in the frame in Figure 5A. Visible Moiré fringes. **(D)** SAED consistent with the ferrite–cementite Bagaryatskii orientation relationship. TEM, 150 kV. LTHAZ, low-temperature heat-affected zone; TEM, transmission electron microscopy, SAED - selected area diffraction pattern

are two varying austenite morphologies (film-like and blocky) characterized by significantly different carbon contents and thus different thermal stabilities. Austenite decomposition products may also be pearlite [22], martensite (induced transformation of retained austenite [23]), and bainite [24]. To evaluate the decomposition products of austenite (and bainitic ferrite) in the LTHAZ, observations of the microstructure were carried out using conventional transmission electron microscopy (TEM) (Figures 5 and 6). It should be noted that the results present the differences between the base material (described by Królicka et al. [9]) and the LTHAZ. The presence of coarse cementite precipitates was found, which usually occurred at the boundaries of the bainitic ferrite laths (Figure 5A and 5B). This proves that filmy austenite decomposed first, which has been confirmed elsewhere in the literature [25]. The presence of Moiré fringes was also identified, which indicates a local misorientation of the crystal lattices (Figure 5C). The orientation of the carbide precipitates and the ferrite matrix was consistent with the typical cementite–ferrite Bagaryatskii relationship – $[111]_\alpha \,||\, [010]_\theta$.

Also, other decomposition products were found in the LTHAZ (Figure 6). Inside the bainitic ferrite laths, carbide precipitates with rod-type and spheroidal-type morphology were identified, which were characterized by various dimensions (Figure 6A). Some of the precipitations also exceeded 300 nm. The base material also contained precipitations inside the laths, but both their fraction and dimensions were significantly lower. Thus, coarsening of carbide precipitates also proves the de-

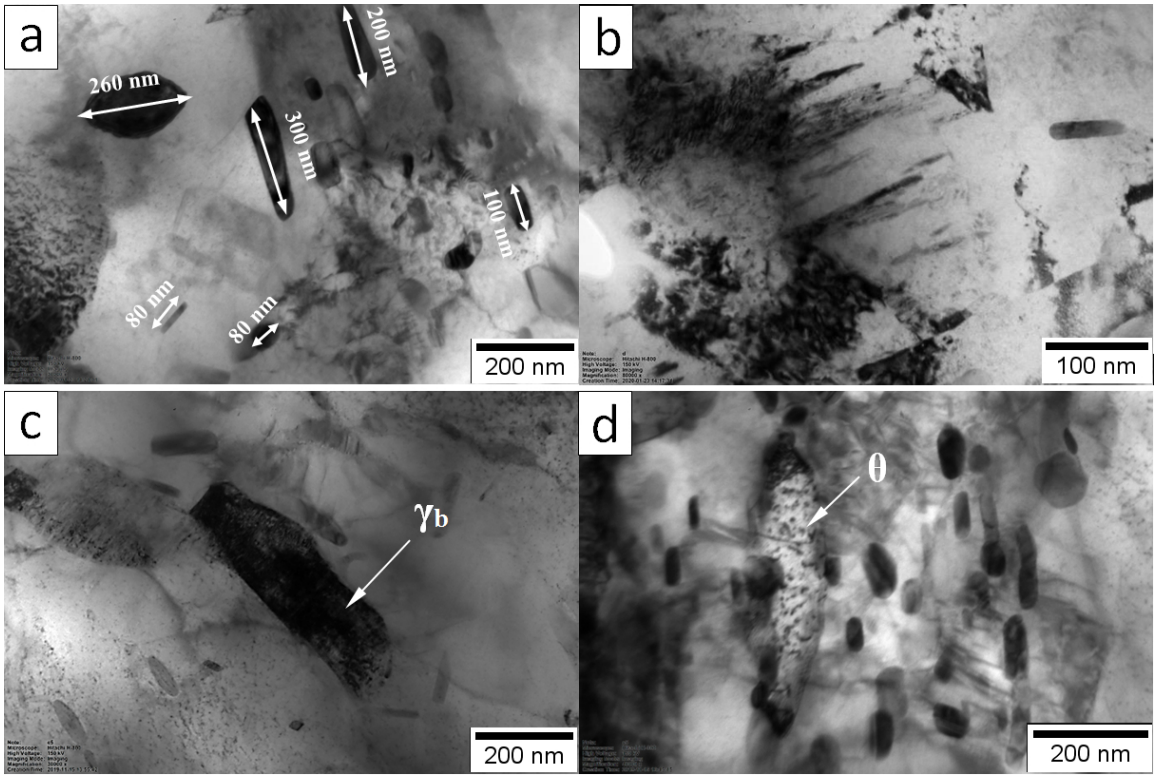

Fig. 6. **(A)** Bright-field image of LTHAZ. Visible coarse cementite precipitations inside bainitic ferrite. **(B)** Upper bainite. **(C)** Refined blocky austenite (γ_b). **(D)** Cementite precipitations (θ) inside refined blocky austenite. TEM, 150 kV. LTHAZ, low-temperature heat-affected zone; TEM, transmission electron microscopy

composition of bainitic ferrite. Locally, upper bainite was identified as a decomposition product of retained austenite (Figure 6B). The presence of refined blocky austenite that did not decompose was also found (Figure 6C). In contrast, blocky austenite characterized by similar dimensions was also identified, which decomposed into a mixture of ferrite and nonmetric cementite (Figure 6D). This indicates that LTHAZ exhibits inhomogeneous decomposition mechanisms that result from the nature of the heat cycles during welding.

It was confirmed by the observations using HRTEM (high-resolution transmission electron microscope) that the coarse carbides are not coherent with the ferrite matrix (Figure 7). Moreover, many dislocations and areas indicating the presence of stress fields were identified. This is an unexpected result because during tempering, the dislocations are removed by recovery, and the tetragonal system disappears (BCT; body-centered tetragonal system)→ BCC; body-centered cubic system) [26]. This can be explained by the presence of residual stresses formed during the welding process. It should also be emphasized that the welding process is much shorter than tempering. Therefore, the recovery phenomenon in the case of welds is limited. Thus, these are major differences between heat-affected zones of welded joints and tempering processes.

As a result of the observation of the carbide at the boundary of the bainitic ferrite lath, it was found that nanometric carbides were also precipitated inside the matrix (Figure 8). Dark-field images from the cementite diffraction reflex indicate that the precipitation process was intensified (Figure 8B and 8D). It can also be emphasized that the dislocations and stress fields were also characterized by a bright contrast (Figure 8B).

To estimate the chemical composition of cementite precipitation, mappings of chemical ele-

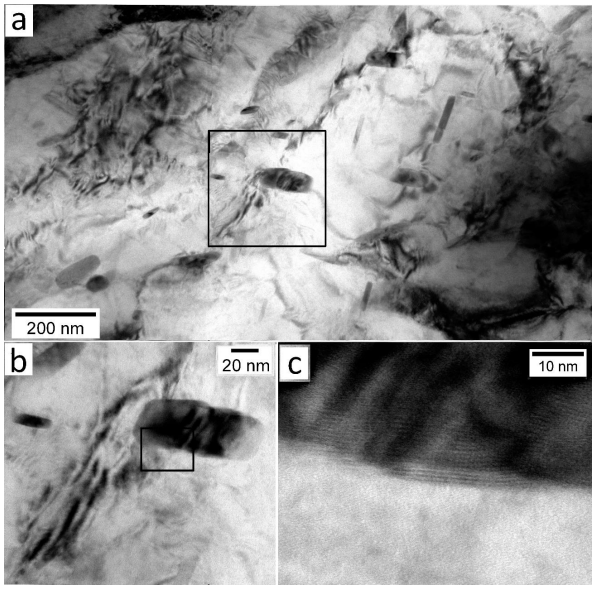

Fig. 7. **(A)** Bright-field image of LTHAZ. Visible cementite precipitations inside bainitic ferrite, dislocations, and areas indicated the stress fields. **(B)** Magnification of coarse cementite precipitations, dislocations, and stress fields. **(C)** Incoherent cementite precipitation with ferrite matrix in the area marked in the frame in Figure 7B. HRTEM, 200 kV. HRTEM, high-resolution transmission electron microscopy; LTHAZ, low-temperature heat-affected zone

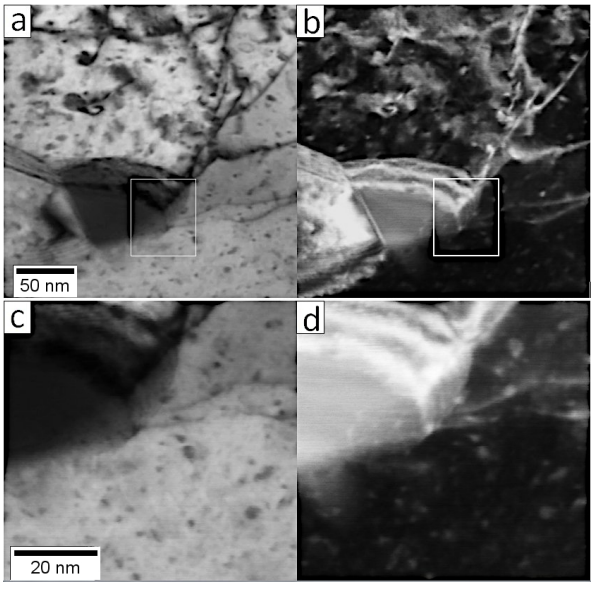

Fig. 8. Bright-field image of LTHAZ **(A)** and corresponding dark-field image from carbides **(B)**. **(C, D)** Magnification of area marked with a frame in Figure 8A and 8B, respectively. HRTEM, 200 kV. HRTEM, high-resolution transmission electron microscopy; LTHAZ, low-temperature heat-affected zone

ments (Si, Cr, and C) were performed (Figure 9). It is known that carbon mapping is characterized by significant measurement uncertainty, but it clearly confirms the presence of carbides (Figure 9B). It is noticeable that the precipitates of carbides are chromium-rich (Figure 9C). In contrast, the distribution of silicon is difficult to assess and appears to be relatively homogeneous (Figure 9D). The weakly visible dominance of silicon in the area of carbides may suggest the presence of orthorhombic iron-rich carbide (FeSi), which was found during the tempering of silicon-rich bainitic steel [27]. However, this hypothesis requires further explanation. Moreover, atom probe field ion microscopy investigations [28] indicate that during tempering, at higher temperatures, the concentration of alloying elements gradually changes (toward equilibrium concentrations) at the ferrite/cementite boundary, and Si diffused out of the carbide. Thus, such a mechanism is also most likely in the LTHAZ.

In summary, the critical LTHAZ is characterized by some differences and similarities with the tempering processes of bainitic steels. Based on the obtained results, the comparison is presented in Table 1. Moreover, optimization of the welding processes may be a prospect for reducing the softening effect in the future. Grajcar et al. [29] indicated that the microstructure morphology of advanced high-strength multiphase steel after laser welding is related to the input energy. It is reasonable that in the case of the flash-but welding method, the reduction of input energy may have a significant impact on the reduction of the critical zone of welded joints of low-carbon bainitic steels. However, this requires further research and consideration in the future, especially in terms of industrial conditions. Also, another prospect is the development of new grades of bainitic steel for continuous cooling processes with enhanced thermal stability [30].

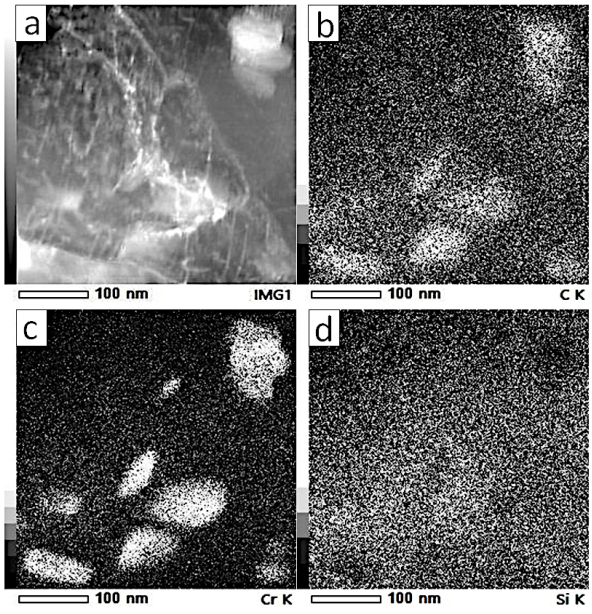

Fig. 9. EDS mapping: **(A)** reference image, **(B)** C concentration, **(C)** Cr concentration, and **(D)** Si concentration. EDS – energy dispersive X-ray spectroscopy

4. Conclusions

- The softening effect in the LTHAZ of welded joints is a critical zone that is responsible for the deterioration in mechanical properties r (hardness drop from 385 HV10 to 275 HV10). The LTHAZ is formed as a result of a short-term exposure to elevated temperature, in which ferrite is still stable (without recrystallization).
- In the LTHAZ of the flash-butt welded joint of low-carbon bainitic rail, severe progress in the decomposition of the retained austenite and bainitic ferrite was identified. The decomposition products of the retained austenite were a mixture of cementite and ferrite and locally upper bainite. Pearlite was not found. The cementite was mainly precipitated at the boundary of the bainitic ferrite laths, which indicates lower thermal stability of the filmy austenite. Moreover, it was found that a part of the refined retained austenite was decomposed into nanometric cementite and ferrite, while another remained in the structure. The decomposition mechanisms are rather heterogeneous in the LTHAZ, and regions with varying degrees of decomposition can be distinguished.
- The carbides precipitated in the bainitic ferrite laths exhibit various dimensions (from several nanometers to 300 nm). They are also characterized by rod-type and spheroidal-type morphologies. Coarsening and an increased amount of carbides indicate the precipitation process from bainitic ferrite and a significant decrease in its carbon content.
- Moiré fringes, as well as a relatively high proportion of dislocations and stress fields, were identified. The reason for their formation is probably the residual stresses arising during the welding process. The levels of residual compressive stresses found in this zone were more than four times higher than the corresponding levels observed in the base material.
- Based on the analysis of these investigations, the capabilities of reducing the critical zone of welded joints were formulated. The first aspect concerns the welding parameters. In this research, typical parameters of welding processes, which are also applied for conventional steels (pearlitic), were used to assess the responsiveness of bainitic steels to welding processes under the same (field) conditions. It should be mentioned that in the case of bainitic steels, the optimal process parameters may be significantly different, and the input energy of the process may play a crucial role. The second aspect is the control of the chemical composition of bainitic steels. It is known that the thermal stability of both retained austenite and bainitic ferrite also depends on the alloying additives. Thus, designing the steel in consideration of the concept of improving thermal stability would allow for a significant reduction in the softening effect.

Acknowledgements

The authors would like to thank JEOL EUROPE for providing access to the high-resolution microscope and Mrs. Liwia Sozańska-Jędrasik for carrying out measurements of residual stresses (Łukasiewicz Research Network – Institute for Ferrous Metallurgy).

Funding

This work was supported by the Polish National Science Centre (Preludium Project, No. 2020/37/N/ST8/03324, title: "The concept of high-strength, thermal stable nanostructured bainitic steel with increased weldability").

References

[1] Hasan SM, Ghosh M, Chakrabarti D, Singh SB. Development of continuously cooled low-carbon, low-alloy, high strength carbide-free bainitic rail steels. Mater Sci Eng A. 2020;771:138590. https://doi.org/10.1016/j.msea.2019.138590

[2] Liu JP, Li YQ, Jin J, Zhang YH, Liu FS, Su R, et al. Effect of processing techniques on microstructure and mechanical properties of carbide-free bainitic rail steels. Mater Today Commun. 2020;25:101531. https://doi.org/10.1016/j.mtcomm.2020.101531

[3] Milenin A, Zalecki W, Pernach M,Rauch Ł, Kuziak R, Zygmunt T, et al. Numerical simulation of manufacturing process chain for pearlitic and bainitic steel rails. Arch Civ Mech Eng. 2020;20:107. https://doi.org/10.1007/s43452-020-00107-0

[4] Adamczyk-Cieślak B, Koralnik M, Kuziak R, Majchrowicz K, Zygmunt T, Mizera J. The impact of retained austenite on the mechanical properties of bainitic and dual phase steels. J Mater Eng Perform. 2022:1–5. https://doi.org/10.1007/s11665-021-06547-w

[5] Chen Y, Ren R, Zhao X, Chen C, Pan R. Study on the surface microstructure evolution and wear property of bainitic rail steel under dry sliding wear. Wear. 2020; 448–449:203217. https://doi.org/10.1016/j.wear.2020.203217

[6] Hu Y, Guo LC, Maiorino M, Liu JP, Ding HH, Lewis R, et al. Comparison of wear and rolling contact fatigue behaviours of bainitic and pearlitic rails under various rolling-sliding conditions. Wear. 2020;460–461:203455. https://doi.org/10.1016/j.wear.2020.203455

[7] Adamczyk-Cieślak B, Koralnik M, Kuziak R, Brynk T, Zygmunt T, Mizera J. Low-cycle fatigue behaviour and microstructural evolution of pearlitic and bainitic steels. Mater Sci Eng A. 2019;747:144–53. https://doi.org/10.1016/j.msea.2019.01.043

[8] Królicka A, Lesiuk G, Radwański K, Kuziak R, Janik A, Mech R, et al. Comparison of fatigue crack growth rate: pearlitic rail versus bainitic rail. Int J Fatigue. 2021:106280. https://doi.org/10.1016/j.ijfatigue.2021.106280

[9] Królicka A, Radwański K, Kuziak R, Zygmunt T, AmbroziakA. Microstructure-based approach to the evaluation of welded joints of bainitic rails designed for high-speed railways. J Constr Steel Res. 2020;175. https://doi.org/10.1016/j.jcsr.2020.106372

[10] Morawiec M, Kik T, Stano S, Różański M, Grajcar A. Numerical simulation and experimental analysis of thermal cycles and phase transformation behavior of laser-welded advanced multiphase steel. Symmetry (Basel). 2022;14:477. https://doi.org/10.3390/sym14030477

[11] Fang K, Yang JG, Liu XS, Song KJ, Fang HY, Bhadeshia HKDH. Regeneration technique for welding nanostructured bainite. Mater Des. 2013;50:38–43. https://doi.org/10.1016/j.matdes.2013.02.019

[12] Królicka A, Radwański K, Janik A, Kustroń P, Ambroziak A. Metallurgical characterization of welded joint of nanostructured bainite: regeneration technique versus post welding heat treatment. Materials (Basel). 2020;13(21), 4841. https://doi.org/10.3390/ma13214841

[13] Wang L, Speer JG. Quenching and partitioning steel heat treatment. Metallogr Microstruct Anal. 2013;2:268–81. https://doi.org/10.1007/s13632-013-0082-8

[14] Withers PJ, Bhadeshia HKDH. Residual stress part 2 – Nature and origins. Mater Sci Technol. 2001;17:366–75. https://doi.org/10.1179/026708301101510087

[15] Hensel J, Nitschke-Pagel T, Dilger K. On welding residual stresses near fatigue crack tips. Adv Mater Res. 2014;996:801–7. https://doi.org/10.4028/www.scientific.net/AMR.996.801

[16] Nitschke-Pagel T, Wohlfahrt H. Residual stresses in welded joints – sources and consequences. Mater Sci Forum. 2002;404–407:215–26. https://doi.org/10.4028/www.scientific.net/MSF.404-407.215

[17] Zhang K, Dong W, Lu S. Finite element and experiment analysis of welding residual stress in S355J2 steel considering the bainite transformation. J Manuf Process. 2021;62:80–9. https://doi.org/10.1016/j.jmapro.2020.12.029

[18] Suikkanen PP, Cayron C, DeArdo AJ, Karjalainen LP. Crystallographic analysis of isothermally transformed bainite in 0.2C-2.0Mn-1.5Si-0.6Cr steel using EBSD. J Mater Sci Technol. 2013;29:359–66. https://doi.org/10.1016/j.jmst.2013.01.015

[19] Caballero FG, Miller MK, Garcia-Mateo C. The approach to equilibrium during tempering of a bulk nanocrystalline steel: an atom probe investigation. J Mater Sci. 2008;43:3769–74. https://doi.org/10.1007/s10853-007-2157-x

[20] Królicka A, Ambroziak A, Żak A. Welding capabilities of nanostructured carbide-free bainite: review of welding methods, materials, problems, and perspectives. Appl Sci. 2019;9:3798. https://doi.org/10.3390/app9183798

[21] Ruiz-Jimenez V, Kuntz M, Sourmail T, Caballero FG, Jimenez JA, Garcia-Mateo C. Retained austenite destabilization during tempering of low-temperature bainite. Appl Sci. 2020;10:8901. https://doi.org/10.

3390/app10248901

[22] Garcia-Mateo C, Peet M, Caballero FG, Bhadeshia HKDH. Tempering of hard mixture of bainitic ferrite and austenite. Mater Sci Technol. 2004;20:814–8. https://doi.org/10.1179/026708304225017355

[23] Sourmail T, Otter L, Collin S, Billet M, Philippot A, Cristofari F, et al. Direct and indirect decomposition of retained austenite in continuously cooled bainitic steels: influence of vanadium. Mater Charact. 2021;173:110922. https://doi.org/10.1016/j.matchar.2021.110922

[24] Fang K, Yang JG, Song KJ, Liu XS, Wang JJ, Fang HY. Study on tempered zone in nanostructured bainitic steel welded joints with regeneration. Sci Technol Weld Join. 2014;19:572–7. https://doi.org/10.1179/1362171814y.0000000227

[25] Saha-Podder A. Tempering of a mixture of bainite and retained austenite. University of Cambridge; 2011.

[26] Caballero FG, Miller MK, Clarke AJ, Garcia-Mateo C. Examination of carbon partitioning into austenite during tempering of bainite. Scr Mater. 2010;63:442–5. https://doi.org/10.1016/j.scriptamat.2010.04.049

[27] Hulme-Smith CN, Lonardelli I, Peet MJ, Dippel AC, Bhadeshia HKDH. Enhanced thermal stability in nanostructured bainitic steel. Scr Mater. 2013;69:191–4. https://doi.org/10.1016/j.scriptamat.2013.03.029

[28] Caballero FG, Miller MK, Garcia-Mateo C, Capdevila C, Babu SS. Redistribution of alloying elements during tempering of a nanocrystalline steel. Acta Mater. 2008;56:188–99. https://doi.org/10.1016/j.actamat.2007.09.018

[29] Grajcar A, Morawiec M, Różański M, Stano S. Twin-spot laser welding of advanced high-strength multiphase microstructure steel. Opt Laser Technol. 2017;92:52–61. https://doi.org/10.1016/j.optlastec.2017.01.011

[30] Królicka A, Żak AM, Caballero FG. Enhancing technological prospect of nanostructured bainitic steels by the control of thermal stability of austenite. Mater Des. 2021;211:110143. https://doi.org/10.1016/j.matdes.2021.110143

Received 2022-03-11
Accepted 2022-04-03